Intermetallics 133 (2021) 107183

Contents lists available at ScienceDirect

Intermetallics

journal homepage: http://www.elsevier.com/locate/intermet

Remarkable increase of Curie temperature in doped GdFeSi compound

A.G. Kuchin [a,*], S.P. Platonov [a], A.V. Lukoyanov [a,b], A.S. Volegov [a,b], V.S. Gaviko [a,b], R. D. Mukhachev [b], M.Yu. Yakovleva [a]

[a] M.N. Miheev Institute of Metal Physics UD RAS, Ekaterinburg, Russia
[b] Ural Federal University Named After B.N. Yeltsin, Ekaterinburg, Russia

ARTICLE INFO

Keywords:
Rare earth compounds
Crystal structure
Magnetic measurements
Electronic structure

ABSTRACT

The $GdFe_{1-x}Ti_xSi$ (x = 0–0.2) intermetallic compounds have been studied. They crystallize into the tetragonal CeFeSi (*P4/nmm*)–type structure. With increasing Ti content, the Curie temperature T_C and the lattice parameter c increase quickly for x = 0–0.1 and then, more moderate because of the solubility limit, whereas the saturation magnetization at 4 K and the lattice parameter a remain almost unchanged. The theoretical DFT + U calculations showed that the growth of Ti content affects the electronic structure of $GdFe_{1-x}Ti_xSi$ by significantly increasing the density of electron states at the Fermi level $N(E_F)$. At the same time, the total magnetic moment does not change because both Fe and Ti are non-magnetic in these intermetallic compounds. The growth of the density of electron states near the Fermi level is accompanied by the rapid growth of T_C in the $GdFe_{1-x}Ti_xSi$ system.

1. Introduction

The RTX family of materials, where R is a rare earth metal, T is a transitional metal and X is a *p*-block element, consists of many compounds with interesting fundamental properties and application potential [1]. Functional magnetic materials such as permanent or soft magnets, magnetostrictive and magnetic shape memory alloys, are very important for modern society. Relevant is the search for new magnetocaloric materials for room temperature application in magnetic refrigerates due to high efficiency, reliability, and environmental safety [2,3]. The GdFeSi and GdTiSi compounds crystallize into the tetragonal CeFeSi (*P4/nmm*)-type structure [4]. In this structure, the rare earth (001) layers are separated by T and Si layers with the sequence: Gd-Si-T2-Si-Gd-Gd-Si-T2-Si-Gd. Therefore, the exchange interactions between atoms Gd–Gd, Gd–T, T–T depend on the lattice parameter c and should weaken with increasing c. The hybridization between Si p states and 3d states of transition metal atom leads to the filling of 3d band and absence of the magnetic moment of Fe or Co in the GdTSi compounds [4–6].

The GdFeSi compound exhibits rather a large value of the magnetocaloric effect MCE of 5.4 J/kg*K in a field of 20 kOe [5]. However, the Curie temperature T_C = 118 K is small for practical application of GdFeSi [5]. GdTiSi is known to order into ferromagnetic state at T_C = 294 K [6]. In order to raise T_C of GdFeSi to room temperature, we partially replace Fe by Ti. Preliminary structural analyses of the $GdFe_{1-x}Ti_xSi$ compounds, as well as magnetic measurements down to T = 90 K were published in conference materials [7]. The solubility limit equals only x ~0.1 (see Table 1 below), since the ratio (1.159) of the atomic radii of Ti (1.46 Å) and Fe (1.26 Å) is large and even slightly exceeds the critical value (1.15) from the Yum-Rosery rule for the formation of such solid solutions [8]. A sharp increase of T_C by 44 K is established when Ti atoms substituted for Fe in the $GdFe_{1-x}Ti_xSi$ compounds only at x = 0.05. The reasons for such a significant specific increase of T_C is unclear. Indeed, the substitution of Ti for Fe sharply increases the interatomic distances and, therefore, should conversely weaken exchange interactions between atoms in the $GdFe_{1-x}Ti_xSi$ system.

In order to understand the reasons for the rapid growth of T_C in the $GdFe_{1-x}Ti_xSi$ compounds and also to confirm this effect, in the present work we performed additional structural studies and measurements of T_C using an alternative method, determined the saturation magnetization of single-crystalline samples at 4 K, and calculated parameters of electronic structure of the compounds.

2. Experimental details

The $GdFe_{1-x}Ti_xSi$ compounds were synthesized by arc melting in an atmosphere of purified argon. Then the alloys were annealed at 1073 K for week and quenched in water. X-ray diffractometer PANalytical of Empyrean Series 2 was used for the structural analysis and lattice parameters determination. Calculations of the lattice parameters and

* Corresponding author.
E-mail address: kuchin@imp.uran.ru (A.G. Kuchin).

https://doi.org/10.1016/j.intermet.2021.107183
Received 28 October 2020; Received in revised form 21 January 2021; Accepted 8 March 2021
Available online 24 March 2021

Table 1
The lattice parameters *a, c* and phase content derived. from Rietveld refinements of the XRD patterns of the $GdFe_{1-x}Ti_xSi$ ($x = 0$, 0.05, 0.1, 0.15, 0.2) alloys. $GdFe_{1-x}Ti_xSi$ are the CeFeSi-type structure, Gd_5Si_3 is the Mn_5Si_3-type structure.

$GdFe_{1-x}Ti_xSi$ (x)	Structural Types	Lattice parameters[a]		Content[b] (%)
		A (Å)	*c* (Å)	
0	CeFeSi	3.999	6.799	92
	Mn_5Si_3	8.484	6.364	8
0.05	CeFeSi	4.007	6.876	92
	Mn_5Si_3	8.509	6.404	8
0.1	CeFeSi	3.984	6.915	82
	Mn_5Si_3	8.476	6.377	18
0.15	CeFeSi	3.990	6.927	~74
	Mn_5Si_3	8.478	6.376	~26
0.2	CeFeSi	3.995	6.935	~58
	Mn_5Si_3	8.485	6.379	~42

[a] The accuracy of determination of the parameters *a, c*: ± 0.001 for $GdFe_{1-x}Ti_xSi$ and ± 0.005 for Gd_5Si_3.
[b] Some extra phases cannot be identified in the compounds with $x = 0.15$, 0.2.

analysis of the phase compositions were carried out in the frame of the HighScore v.4.x programs. The ingots contain single-crystals weighing of about 1–3 mg. These single-crystalline specimens were oriented by the Laue X-ray back-reflection method. Stereograms for determining the orientation of the crystal axes were calculated using the CaRine program (http://carine.crystallography.pagespro-orange.fr). MPMS was used for magnetic study in an applied magnetic field of strength up to 70 kOe and in the temperature range 4–300 K. The magnetization curves *M(H)* were measured along the main crystallographic directions [100], [010] and [001] of the single-crystals. The saturation magnetization M_{sat} at 4 K was determined by the linear extrapolation of the high-field part of the *M(H)* curves measured on free powder samples or along the easy-magnetization axis of single-crystals to zero inverse field ($1/H$). The temperatures of the magnetic phase transitions in the samples were determined from the magnetization vs. temperature $M(T)$ curves in a field of 100 Oe. Before measuring $M(T)$, the samples were cooled from 300 to 4 K in the absence of external field.

3. Experimental results and discussion

3.1. Crystal structure

The $GdFe_{1-x}Ti_xSi$ compounds crystallize into the tetragonal CeFeSi (*P4/nmm*)–type structure. A parasitic Gd_5Si_3 phase with a hexagonal Mn_5Si_3 (*P6*$_3$*/mcm*)–type structure is also presented in the alloys. Fig. 1 shows the experimental and calculated X-ray diffraction patterns for $GdFe_{0.9}Ti_{0.1}Si$. The additional reflections from Gd_5Si_3 are taken into account in simulations. The phase content of the $GdFe_{1-x}Ti_xSi$ alloys is summarized in Table 1. It can be seen that the content of the main CeFeSi–type phase decreases rapidly with increasing titanium content in the alloy, *i.e.*, the mutual solubility of GdFeSi and GdTiSi compounds rapidly decreases. In the alloys with $x = 0.15$, 0.2 it is not possible to accurately determine the content of the main phase because of the presence of unidentified extra phases.

The increase in the Ti content in the $GdFe_{1-x}Ti_xSi$ system results in a quick increase in the lattice parameter *c* for $x = 0$–0.1 and then slow increase for $x = 0.1$–0.2, in accordance with the rapid decrease of the mutual solubility of GdFeSi and GdTiSi compounds (Table 1). The change of the lattice parameter *a* is negligible (Table 1).

Back-reflection Laue patterns of single crystals of the GdFeSi and $GdFe_{0.95}Ti_{0.05}Si$ compounds are shown in Figs. 2 and 3. The main crystallographic directions [001], [010] and [100] are marked. Points from the experimental back-reflection Laue patterns in Figs. 2 and 3 fit well with the back-reflection Laue patterns calculated from the stereographic projections for the (001) and (100) planes of the tetragonal phase of the GdFeSi and $GdFe_{0.95}Ti_{0.05}Si$ compounds, respectively.

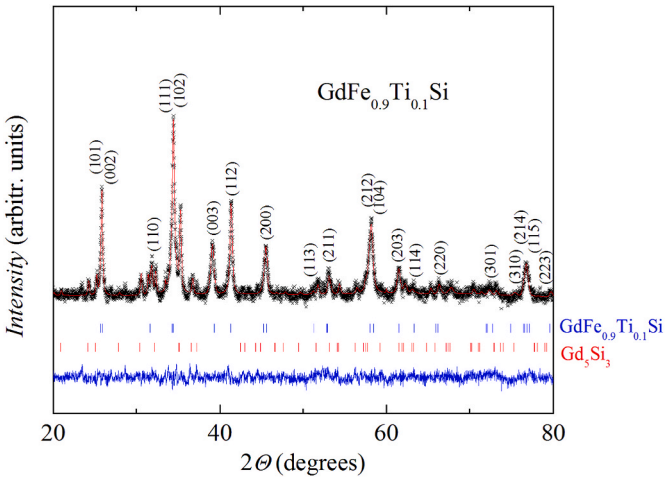

Fig. 1. X-ray diffraction pattern (symbols) of the $GdFe_{0.9}Ti_{0.1}Si$. alloy and its fitting by envelop curve. The difference between the experimental and the calculated results is shown by the lower curve. Vertical lines show the reflection positions for the (up-down) $GdFe_{0.9}Ti_{0.1}Si$ and Gd_5Si_3 compounds. Indexes are presented for the CeFeSi-type structure (for the $GdFe_{0.9}Ti_{0.1}Si$ compound).

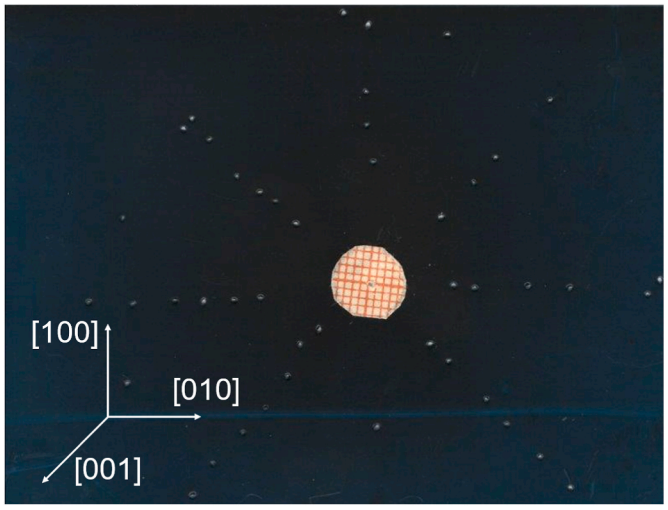

Fig. 2. Back-reflection Laue pattern of the GdFeSi. single crystal. The [001] axis is directed along the X-ray beam and perpendicular to the plane of the pattern. The [100] and [010] axes are located vertically and horizontally, respectively.

3.2. Magnetic properties

The Curie temperatures T_C of the $GdFe_{1-x}Ti_xSi$ compounds are presented in Table 2. They were determined as the minimum value of the first derivative of the $M(T)$ dependences in a field of 100 Oe presented in Fig. 4. The values of T_C determined in this way are close to those obtained with the help of Arrott-Belov plots in Ref. [7]. The Curie temperature of the $GdFe_{1-x}Ti_xSi$ compounds increases quickly in the range $x = 0$–0.1 and then more moderate for $x = 0.1$–0.2 (Table 2). The concentration dependence of the T_C is similar to that of the lattice parameter *c*, it also shows that the solubility limit is somewhere above x ~0.1. The blurred kink in the $M(T)$ curves corresponding to the ferromagnet-to-paramagnet transition for the $GdFe_{1-x}Ti_xSi$ substitutional alloys, in comparison with the initial GdFeSi compound, confirms their strong heterogeneity, which was assumed in Ref. [7]. In addition to the ferromagnet-to-paramagnet transition in the main phase in the range $T = 130$–190 K, a step appears on the $M(T)$ dependences at T below 90 K,

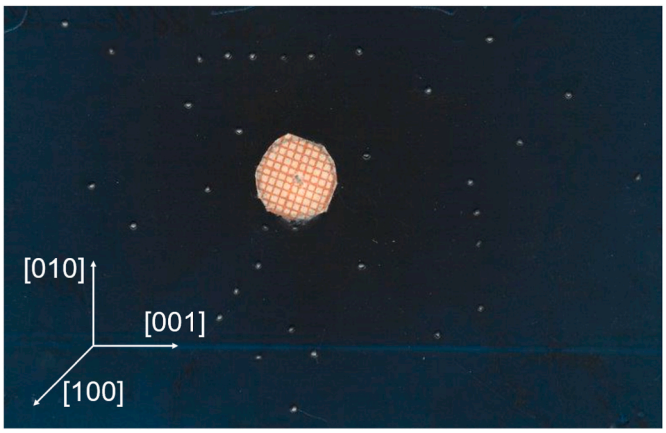

Fig. 3. Back-reflection Laue pattern of the $GdFe_{0.95}Ti_{0.05}Si$ single crystal. The [100] axis is directed along the X-ray beam and perpendicular to the plane of the figure. The [010] and [001] axes are located vertically and horizontally, respectively.

Table 2
The Curie temperature T_C and saturation. magnetization $M_{sat.}$ at $T = 4$ K for the $GdFe_{1-x}Ti_xSi$ compounds, $x = 0$, 0.05, 0.1, 0.15, 0.2.

$GdFe_{1-x}Ti_xSi$ (x)	T_C (K)	$M_{sat.}$[a] (μ_B/f.u.)
0	124.5	7.0
0.05	168	7.1
0.1	182	6.9
0.15	186.4	~7.3
0.2	188.6	–

[a] Some extra phases cannot be identified in the compounds with $x = 0.15$, 0.2.

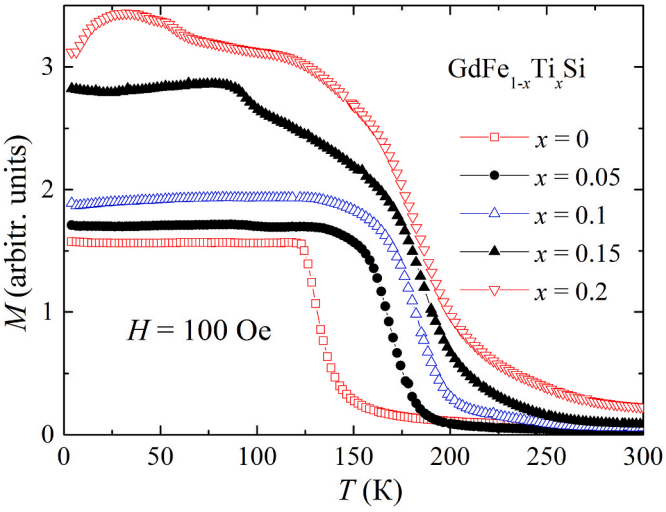

Fig. 4. Temperature dependences of the magnetizations. of the $GdFe_{1-x}Ti_xSi$ compounds with $x = 0$, 0.05, 0.1, 0.15, 0.2 measured in a field of 100 Oe.

which can be attributed to the antiferromagnet-to-paramagnet transition in the parasitic Gd_5Si_3 phase, modified in the molecular magnetic field of the main ferromagnetic phase. According to the published data, the Gd_5Si_3 phase is characterized by the Néel temperature $T_N = 55$ K or 75 K [9,10]. A much more complex $M(T)$ dependence with possible several additional magnetic phase transitions is observed for the alloy with $x = 0.2$, for which the content of the main phase is minimal and some additional parasitic phases cannot be identified by X-ray diffraction (Table 1).

Magnetization curves of the GdFeSi and $GdFe_{0.95}Ti_{0.05}Si$ single crystals at $T = 4$ K are presented in Figs. 5 and 6, respectively. The back-reflection Laue patterns of these crystals are shown in Figs. 2 and 3. GdFeSi is easily magnetized along the [001] axis and heavily magnetized in the basal plane where magnetic anisotropy is absent. The anisotropy field in GdFeSi equals ~7.8 kOe at $T = 4$ K (Fig. 5) and ~3.8 kOe at 90 K [7]. The magnetic anisotropy vanishes in $GdFe_{0.95}Ti_{0.05}Si$ and $GdFe_{0.9}Ti_{0.1}Si$, as is shown for $GdFe_{0.95}Ti_{0.05}Si$ in Fig. 6. This disappearance of magnetic anisotropy in the $GdFe_{1-x}Ti_xSi$ substitution compounds can be caused by chaotic localization of crystal electric fields arising due to different electric charges of Ti and Fe ions.

The saturation magnetizations $M_{sat.}$ at $T = 4$ K of the $GdFe_{1-x}Ti_xSi$ compounds are shown in Table 2. It can be seen that for the alloys with $x = 0$–0.1, for which all phases are determined from X-ray diffraction, $M_{sat.}$ equals to 6.9–7.0 μ_B/f.u. For the composition $x = 0.15$ $M_{sat.}$~7.3 μ_B/f.u., which differs from the values of $M_{sat.}$ for $x = 0$–0.1 by an amount close to the measurement error of 2–3%. That is, the contribution of undetermined phases to the magnetism of the alloy $x = 0.15$ is insignificant. The practical constancy of $M_{sat.}$ ~7.0 μ_B/f.u. for the compounds $x = 0$–0.1 does not contradict the fact that Ti and Fe ions are non-magnetic in the initial ternary compounds of the system. The results of band calculations also confirm the invariability of the saturation magnetization in the $GdFe_{1-x}Ti_xSi$ compounds (see Section 4.2.). The close value $M = 7.1$ μ_B/f.u. at 4.2 K and in 20 kOe field was obtained for GdFeSi in Ref. [4]. It is obvious that the invariable saturation magnetization cannot cause the rapid increase of T_C in the $GdFe_{1-x}Ti_xSi$ compounds. Therefore, we decide to study parameters of the electronic structure of the $GdFe_{1-x}Ti_xSi$ compounds to understand the rise of their T_C.

4. Calculations of the electronic structure and magnetic moments. Curie temperature interpretation

4.1. Calculation method

The electronic structure of the $GdFe_{1-x}Ti_xSi$ intermetallic compounds was calculated with the DFT + U method [11] in the Quantum ESPRESSO software package [12] using the exchange-correlation potential in the generalized gradient approximation (GGA) of the Perdew-Burke-Ernzerhof (PBE) version [13]. Wave functions were decomposed into plane waves, and interactions between ions and valence electrons were taken into account in the framework of projector

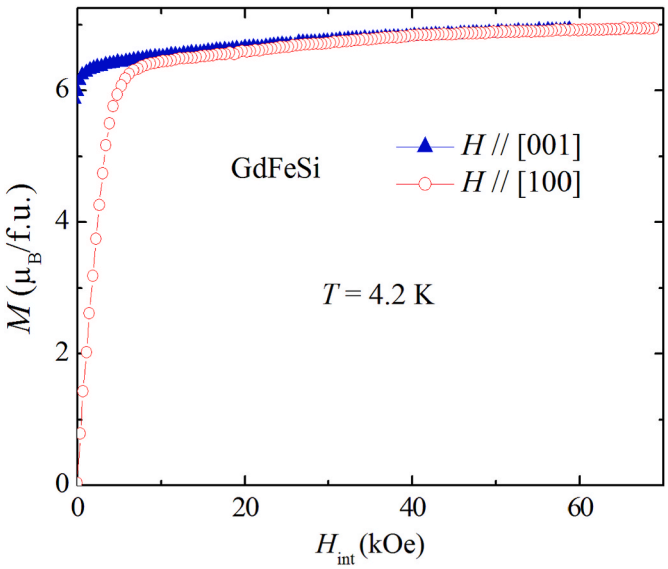

Fig. 5. Magnetization curves versus internal field measured along the crystallographic directions [001] (▲) and [100] (○). of the GdFeSi single crystal at $T = 4$ K.

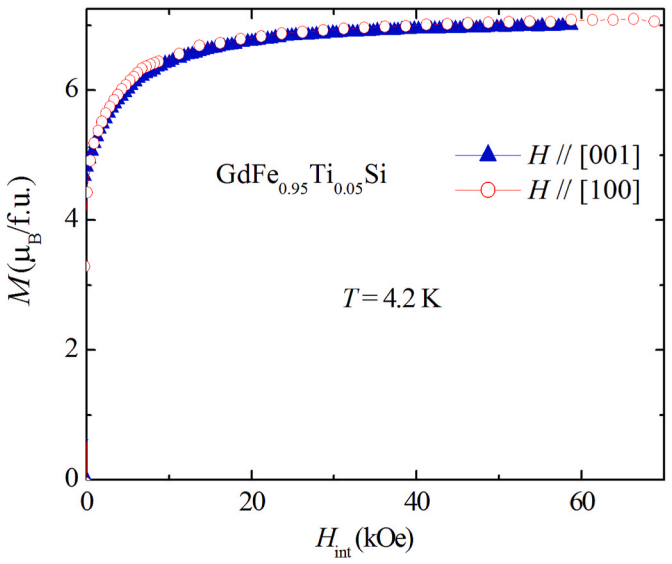

Fig. 6. Magnetization curves versus internal field measured along the crystallographic directions [001] (▲) and [100] (○) of the $GdFe_{0.95}Ti_{0.05}Si$ single crystal at $T = 4$ K.

augmented wave method (PAW). PAW potentials were used in the calculations for Gd from the set of rare-earth potentials from work [14], for Fe and Si from standard Quantum ESPRESSO library obtained from the ATOMPAW program [15]. To achieve sufficient convergence in the self-consistency cycle, an energy cut-off for plane waves equal to 60 Ry was taken. Integration in reciprocal space was performed using a grid of $8 \times 8 \times 8$ k-points. Spin-orbit coupling was not taken into account in our calculations because only the collinear arrangement of magnetic moments was found for the considered compounds (see Section 3.2). To account for strong electronic correlations in the Gd 4*f* electronic shell, the DFT + U correction was included for the parameters of direct Coulomb $U = 6.7$ eV and exchange (Hund) $J_H = 0.7$ eV interactions. These values are widely used for the Gd ions in different intermetallic compounds [11,16].

4.2. Calculation results and discussion

For the electronic structure calculations of the experimental crystal structure parameters reported in Section 3.1 were used. In the self-consistent calculations using the DFT + U method, the iron and silicon ions remain almost non-magnetic with the magnetic moments 0.01 μ_B for Si and 0.003 μ_B for Fe, respectively. For the Gd ions, the calculated DFT + U spin polarization corresponds to the magnetic moment of about 7.2 μ_B per rare-earth ion and formula unit, see Table 3. This is close to the experimental result $M_{sat.}$~6.9–7.0 μ_B/f.u. presented in section 3.2 for the $GdFe_{1-x}Ti_xSi$, $x = 0$–0.1 compounds.

Table 3
Calculated parameters for $GdFe_{1-x}Ti_xSi$, $x = 0$–0.2: the values of the rigid-band shift, the magnetic moment value of the Gd ion, the total and partial spin densities of states DOS at the Fermi energy E_F.

$GdTi_xFe_{1-x}Si$ (x)	Shift value (eV)	Magnetic moment of Gd ion (μ_B)	Majority spin DOS value at E_F (st./eV*f.u.)	Minority spin DOS value at E_F (st./eV*f.u.)	Total DOS value at E_F (st./eV*f.u.)
0	0	7.21	1.57	1.74	3.31
0.05	−0.06	7.22	1.63	1.92	3.55
0.1	−0.12	7.22	1.73	2.10	3.83
0.15	−0.19	7.22	1.82	2.20	4.02
0.2	−0.26	7.22	1.98	2.32	4.30

In $GdFe_{1-x}Ti_xSi$, to take into account the Ti-doping of 5, 10, 15, and 20%, the rigid band shift method was employed for the experimental crystal structure parameters taken for the corresponding chemical compositions. Then, the Fermi energy was shifted to account for the changed number of electrons in the 3*d* metals in $GdFe_{1-x}Ti_xSi$ according to the experimental chemical composition of Fe and Ti (Table 3).

In Fig. 7, the densities of electron states N per formula unit for the GdFeSi intermetallic compound are given for the majority and minority spins. The Fermi energy E_F is set to zero of energy. Several localized bands of varying intensity form the intense peaks in the electronic structure of GdFeSi. In the energies about −7 eV below and 5 eV above the Fermi energy level, the well-localized Gd 4*f* states are located. Near E_F from −5 to 3 eV the electronic structure is formed by the wide non-spin-polarized bands of the Fe 3*d* and Si 3*p* electronic states. All other electronic states have minor contribution to this energy range. The electronic states for the $GdFe_{1-x}Ti_xSi$ composition with $x = 0.2$ are shown in Fig. 8. The rigid band shift in this case equals to −0.26 eV to account for the 20% Ti-doping. Despite the small value of the shift when the Ti doping is taken into account, the total and partial spin DOS at the E_F increase (see Table 3), because it is shifted to the slope of the nearest peaks of the DOS (Figs. 7 and 8).

A decrease in the number of 3*d* electrons in both subbands of the non-spin-polarized 3*d* band (Figs. 7 and 8) does not lead to the formation of a moment in the 3*d* band when iron is replaced by titanium in $GdFe_{1-x}Ti_xSi$. Changes in the density of states at the Fermi level caused by the mutual substitution of 3*d* metals do not affect the well-localized Gd 4*f* states (Figs. 7 and 8) and, for this reason, the magnetic moment of the Gd ion remains unchanged in the $GdFe_{1-x}Ti_xSi$ system (Table 3). As a result, the magnetic moment of the $GdFe_{1-x}Ti_xSi$ compounds is equal to the moment of the Gd ion for all compositions.

4.3. Curie temperature interpretation

To explain the rapid growth of the T_c with x for the $GdFe_{1-x}Ti_xSi$

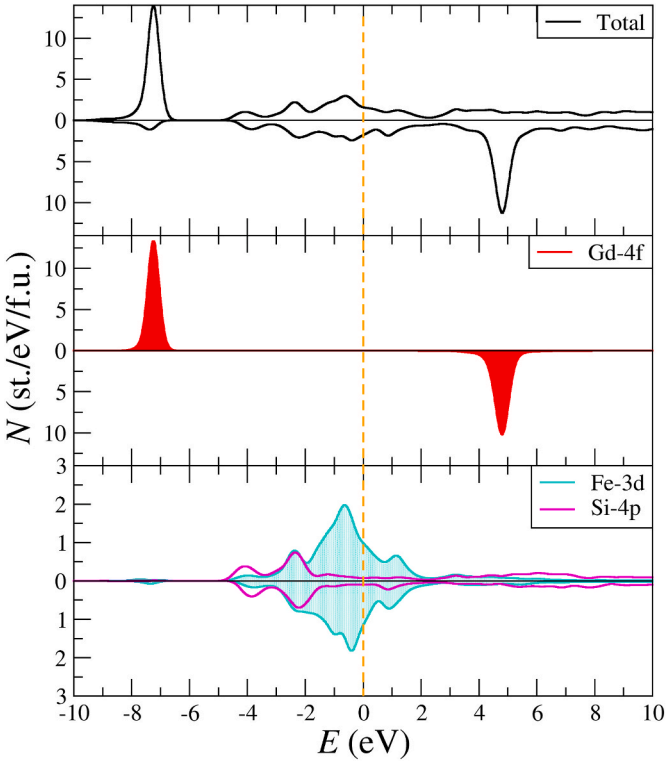

Fig. 7. Total and partial densities of electron states N of GdFeSi. The Fermi energy E_F is shown as a dashed line at zero energy.

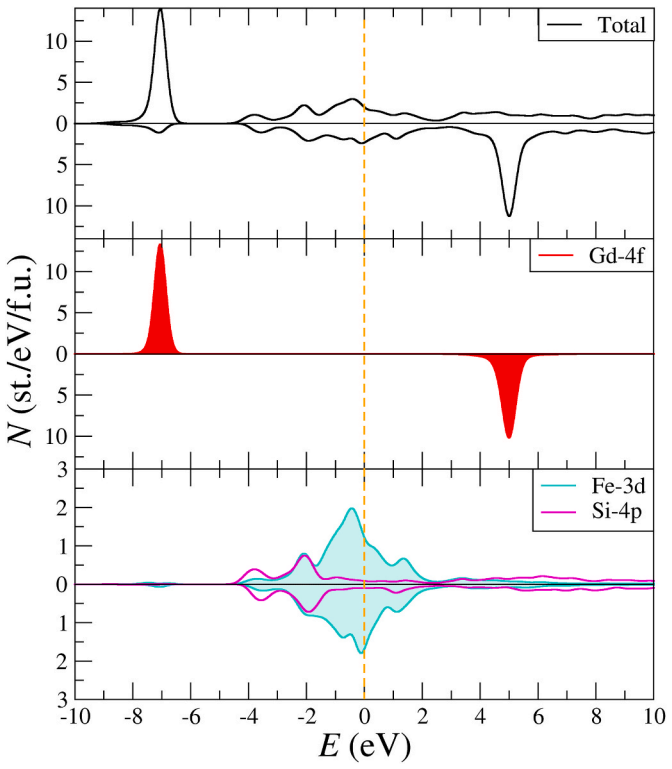

Fig. 8. Total and partial densities of electron states N of $GdFe_{0.8}Ti_{0.2}Si$. The Fermi energy E_F is shown as a dashed line at zero energy.

ferromagnets, we used a model of effective d–f exchange interaction in R-3d metal intermetallics [17,18] that describes the indirect f–f exchange between the R ions:

$$T_c \sim G^* \Gamma^{2*}\chi_{Fe} \sim \Gamma^{2*}\chi_{Fe} \sim \Gamma^{2*}N(E_F) \quad (1)$$

Here, G is the de Gennes factor for the Gd ion, Γ is the effective constant of the effective d–f exchange interactions, χ_{Fe} is the susceptibility of the Fe mixed 3d-band for the $GdFe_{1-x}Ti_xSi$ ferromagnets, $N(E_F)$ is the DOS at the Fermi level. Γ is a weakly changing function of the filling degree of the Fe 3d-band.

The Inset in Fig. 9 shows the concentration dependences of the Curie temperature and total DOS at the Fermi level $N(E_F)$ for the $GdFe_{1-x}Ti_xSi$ system. It is seen that both parameters increase with increasing titanium content. That is, the increase of $N(E_F)$ can cause the increase of T_c, in accordance with (1). The dependence of T_C on $N(E_F)$ for the $GdFe_{1-x}Ti_xSi$ system is shown in Fig. 9. The $N(E_F)$ grows approximately linearly, while T_C tends to saturation caused by the solubility limit somewhere above $x \sim 0.1$ (see Section 3.1). Probably, the potential for a maximum increase of T_C, stipulated by the monotonic increase of $N(E_F)$, is not realized in the $GdFe_{1-x}Ti_xSi$ system because of the solubility limit $x \sim 0.1$ which is caused by the large size of the Ti atom compared to the Fe atom. We will check this assumption in the case of other 3d elements with atomic radius smaller than that of Ti.

5. Conclusions

In the $GdFe_{1-x}Ti_xSi$, x = 0–0.2 system, when the content of Ti increases, the Curie temperature and interatomic distances increase, whereas the saturation magnetization at 4 K is almost unchanged, as is confirmed by the band structure calculations. The calculations of the electronic structure indicate the increase in the density of electron states at the Fermi level $N(E_F)$ in $GdFe_{1-x}Ti_xSi$ with the Ti content growth. The electronic structure changes in $GdFe_{1-x}Ti_xSi$, resulting in the significant increase of $N(E_F)$, can be a reason for the rapid growth of T_C in the $GdFe_{1-x}Ti_xSi$ system, according to the model of effective d–f exchange interaction in R-3d metal intermetallics. Probably, the potential for a maximum increase of T_c, stipulated by the monotonic increase of $N(E_F)$, is not realized in the $GdFe_{1-x}Ti_xSi$ system because of the solubility limit $x \sim 0.1$, but it can be realized for 3d substitutional elements with an atomic radius smaller than that of Ti.

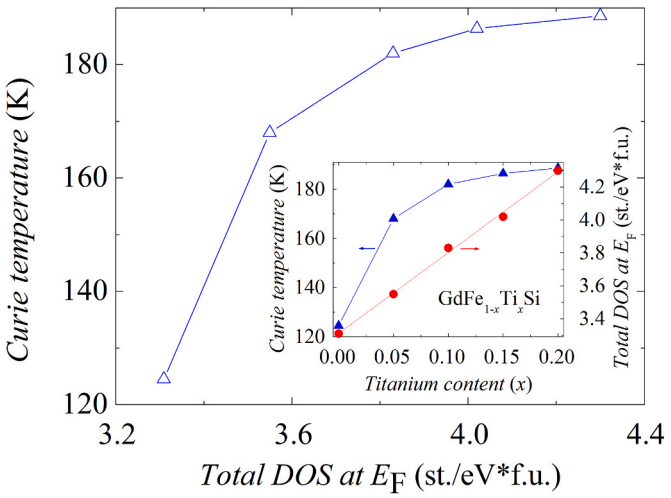

Fig. 9. Curie temperature versus total density of electron states DOS at the Fermi level E_F of the $GdFe_{1-x}Ti_xSi$ system. Inset: Curie temperature and total DOS at the Fermi level of the $GdFe_{1-x}Ti_xSi$ system versus Ti content.

Author statement

A.G. Kuchin: Conceptualization, Supervision, Writing – Original Draft, Writing- Reviewing and Editing.
S.P. Platonov: Investigation, Data curation.
A.V. Lukoyanov: Supervision, Methodology, Software, Writing – Original Draft.
A.S. Volegov: Investigation.
V.S. Gaviko: Investigation, Formal analysis.
R.D. Mukhachev: Software.
M.Yu. Yakovleva: Investigation, Visualization.

Declaration of competing interest

The authors declare that they have no known competing financial interests or personal relationships that could have appeared to influence the work reported in this paper.

Acknowledgements

X-ray diffraction and magnetometric measurements were conducted on equipment of the Collaborative Access Center "Testing Center of Nanotechnologies and Advanced Materials" of the Institute of Metal Physics (Ural Branch, Russian Academy of Sciences). The results of sections 1-3 were obtained within the grant of the Russian Science Foundation (project No. 18-72-10098). The results of section 4 were obtained within the state assignment of Ministry of Science and Higher Education of the Russian Federation (themes "Magnet" No. AAAA-A18-118020290129-5 and "Electron" No. AAAA-A18-118020190098-5).

References

[1] S. Gupta, K. Suresh, Review on magnetic and related properties of RTX compounds, J. Alloys Compd. 618 (2015) 562–606, https://doi.org/10.1016/j.jallcom.2014.08.079.
[2] O. Tegus, E. Brück, K.H.J. Buschow, F. de Boer, Transition-metal-based magnetic refrigerants for room-temperature applications, Nature 415 (2002) 150–152, https://doi.org/10.1038/415150a.

[3] V. Pecharsky, K. Gschneidner, Giant magnetocaloric effect in $Gd_5(Si_2Ge_2)$, Phys. Rev. Lett. 78 (1997) 4494–4497, https://doi.org/10.1103/PhysRevLett.78.4494.
[4] R. Welter, G. Venturini, B. Malaman, Magnetic properties of RFeSi (R≡La-Sm, Gd-Dy) from susceptibility measurements and neutron diffraction studies, J. Alloys Compd. 189 (1992) 49–58, https://doi.org/10.1016/0925-8388(92)90045-B.
[5] P. Wlodarczyk, L. Hawelek, P. Zackiewicz, T. Roy, A. Chrobak, M. Kaminska, A. Kolano-Burian, J. Szade, Characterization of magnetocaloric effect, magnetic ordering and electronic structure in the $GdFe_{1-x}Co_xSi$ intermetallic compounds, Mater. Chem. Phys. 162 (2015) 273–278, https://doi.org/10.1016/j.matchemphys.2015.05.067.
[6] G. Skorek, J. Deniszczyk, J. Szade, B. Tyszka, Electronic structure and magnetism of ferromagnetic GdTiSi and GdTiGe, J. Phys. Condens. Matter 13 (2001) 6397–6409, https://doi.org/10.1088/0953-8984/13/29/309.
[7] A. Kuchin, S. Platonov, V. Gaviko, M. Yakovleva, Magnetic and structural properties of $GdFe_{1-x}Ti_xSi$, IEEE Magnet. Lett. 10 (2019) 2509204, https://doi.org/10.1109/LMAG.2019.2955052.
[8] W.B. Pearson, The Crystal Chemistry and Physics of Metals and Alloys, Wiley, New York, 1972.
[9] F. Canepa, S. Cirafici, M. Napoletano, Magnetic properties of Gd_5T_3 intermetallic compounds (T = Si, Ge, Sn), J. Alloys Compd. 335 (2002) L1–L4, https://doi.org/10.1016/S0925-8388(01)01802-3.
[10] J. Roger, V.S. Babizhetskii, K. Hiebl, J.F. Halet, R. Guérin, Structural chemistry, magnetism and electrical properties of binary Gd silicides and Ho_3Si_4, J. Alloys Compd. 407 (2006) 25–35, https://doi.org/10.1016/j.jallcom.2005.06.038.
[11] V. Anisimov, F. Aryasetiawan, A. Lichtenstein, First-principles calculations of the electronic structure and spectra of strongly correlated systems: the LDA + U method, J. Phys. Condens. Matter 9 (1997) 767–808, https://doi.org/10.1088/0953-8984/9/4/002.
[12] P. Giannozzi, O. Andreussi, T. Brumme, O. Bunau, M.B. Nardelli, M. Calandra, R. Car, C. Cavazzoni, D. Ceresoli, M. Cococcioni, N. Colonna, I. Carnimeo, A. Dal Corso, S. de Gironcoli, P. Delugas, R.A. DiStasio Jr., A. Ferretti, A. Floris, G. Fratesi, G. Fugallo, R. Gebauer, U. Gerstmann, F. Giustino, T. Gorni, J. Jia, M. Kawamura, H.-Y. Ko, A. Kokalj, E. Küçükbenli, M. Lazzeri, M. Marsili, N. Marzari, F. Mauri, N. L. Nguyen, H.-V. Nguyen, A. Otero-de-la-Roza, L. Paulatto, S. Poncé, D. Rocca, R. Sabatini, B. Santra, M. Schlipf, A.P. Seitsonen, A. Smogunov, I. Timrov, T. Thonhauser, P. Umari, N. Vast, X. Wu, S. Baroni, Advanced capabilities for materials modelling with Quantum ESPRESSO, J. Phys. Condens. Matter 29 (2017) 465901, https://doi.org/10.1088/1361-648X/aa8f79.
[13] J. Perdew, K. Burke, M. Ernzerhof, Generalized gradient approximation made simple, Phys. Rev. Lett. 77 (1996) 3865–3868, https://doi.org/10.1103/PhysRevLett.77.3865.
[14] M. Topsakal, R. Wentzcovitch, Accurate projected augmented wave (PAW) datasets for rare-earth elements (RE = La–Lu), Comput. Mater. Sci. 95 (2014) 263–270, https://doi.org/10.1016/j.commatsci.2014.07.030.
[15] N. Holzwarth, A. Tackett, G. Matthews, A Projector Augmented Wave (PAW) code for electronic structure calculations, Part I: atom paw for generating atom-centered functions, Comput. Phys. Commun. 135 (2001) 329–347, https://doi.org/10.1016/S0010-4655(00)00244-7.
[16] S. Gupta, K. Suresh, A. Lukoyanov, Effect of complex magnetic structure on the magnetocaloric and magneto-transport properties in GdCuSi, J. Mater. Sci. 50 (2015) 5723–5728, https://doi.org/10.1007/s10853-015-9116-8.
[17] A. Cyrot, M. Lavagna, Density of states and magnetic properties of the rare-earth compounds RFe_2, RCo_2 and RNi_2, J. Phys. 40 (1979) 763–771, https://doi.org/10.1051/jphys:01979004008076300.
[18] G. Fischer, A. Meyer, Indirect exchange in molecular field model, Solid State Commun. 16 (1975) 355–357, https://doi.org/10.1016/0038-1098(75)90086-1.